


Spatio-temporal monitoring of the iceberg D28 using SCATSAT-1 data

Khoisnam Nanaoba Singh¹, Mamata Maisnam¹, Rajkumar Kamaljit Singh² , Jayaprasad Pallipad³, Arundhati Misra³ and Saroj Maity³

¹National Institute of Technology Manipur, Imphal-795004, India; ²Manipur Technical University, Imphal-795004, India and ³Space Applications Centre – ISRO, Ahmedabad-380015, India

Note

Cite this article: Singh KN, Maisnam M, Singh RK, Pallipad J, Misra A, and Maity S. Spatio-temporal monitoring of the iceberg D28 using SCATSAT-1 data. *Polar Record* 59(e15): 1–6. <https://doi.org/10.1017/S0032247423000062>

Received: 21 August 2022

Revised: 23 March 2023

Accepted: 23 March 2023

Keywords:

Iceberg; D28; SCATSAT-1; Wind; Ocean current; Sea ice

Author for correspondence:

Rajkumar Kamaljit Singh,
Email: kamaljit.rajkumar@gmail.com

Abstract

The study of the icebergs and their movements is one of many applications of scatterometer data in the study of the ecosystems of polar regions. SCATSAT-1 is the Indian Space Research Organisation's (ISRO's) Ku-band (13.515625 GHz) scatterometer. Using enhanced resolution Gamma0H (horizontally polarised incidence angle normalised backscattering coefficient) data of SCATSAT-1, we observed the movement of iceberg D28 and its interaction with wind, ocean currents and sea ice for one and a half years of its journey (JD 269, 2019 to JD 051, 2021). The data sets used are as follows: (1) SCATSAT-1 level-4 Gamma0H; (2) OSCAR (Ocean Surface Current Analysis Real-time) third-degree resolution ocean surface currents; (3) hourly wind speed data of ERA5; 4) NSIDC (National Snow and Ice Data Center) sea ice concentration data; and (5) NSIDC Polar Path-finder Daily EASE-Grid Sea Ice Motion Vectors, Version-3. For this study, we divide the continent into five different regions/sectors. It is found that the trajectory of the iceberg is influenced by the resultant of the wind and ocean current, at different scales in these regions. Moreover, sea ice motion can also change the course of iceberg. From the on-screen digitisation of the iceberg, the average area of the iceberg is found to be approximately 1509.82 km² with approximate dimensions of 27 km × 55.5 km. We conclude that spatial and temporal behaviours of the iceberg can be ascertained from the scatterometer data.

Introduction

Tracking and predicting iceberg drift trajectories has important implications for voyages near polar regions. Since 1978, using Synthetic Aperture Radar (SAR), visible, and infrared remotely sensed imageries, the US National Ice Centre (US NIC) has been tracking Antarctic icebergs (<https://usicecenter.gov/Resources/AntarcticIcebergs>). Using scatterometer and radiometer data, the Microwave Earth Remote Sensing (MERS) group at the Brigham Young University (BYU) analyses and archives Antarctic iceberg tracks from 1992 till date (Ballantyne & Long, 2002).

The study of iceberg drag is performed by developing models and statistical relationships with drag forces (wind drag, ocean current drag, sea ice drags, etc.). Sea ice provides an important drag force in the study of Antarctic giant iceberg dynamics (Hunke & Comeau, 2011; Lichey & Hellmer, 2001). The influence of wind, ocean current and towing forces on icebergs is further typically studied by developing numerical models (Crépon, Houssais & Saint, 1988; Smith & Banke, 1983; Wagner, Dell, & Eisenman, 2017; Wesche & Dierking, 2016)

Applications for scatterometer satellite data in cryospheric investigations include mapping snow cover, ice types and extent, tracking icebergs, and observing sea ice motion and melting (Long, 2016; Singh, Tiwari, Sood, Kaur & Prashar, 2022). The iceberg tracking database on the BYU website is made from enhanced scatterometer data (Ballantyne & Long, 2002).

The Indian Space Research Organisation's (ISRO) Ku-band (13.515 GHz) scatterometer was launched on 26 September 2016 from ISRO's space-port Sriharikota on-board the PSLV C35 mission (Misra et al., 2019). It has been used in three main categories of studies: (1) ocean dynamics; (2) cryospheric studies; and (3) agriculture and land hydrology (Oza et al., 2019; Singh, Tiwari, Gusain, & Sood, 2020). The capability of the SCATSAT-1 to detect ice shelf calving events and iceberg edges was shown by Singh et al. (2021). As an extension to Singh et al. (2021), in this study we used SCATSAT-1 scatterometer data to observe and track the D28 iceberg, which calved from the Amery Ice Shelf.

The objectives of the study can be summarised as: (1) tracking and calculation of the trajectory of the iceberg from digitisation, and (2) observation of its movement under different wind, ocean, and sea ice conditions.

Data

We used four parameters that affect the movement of the iceberg, namely wind velocity, ocean surface current, sea ice concentration and sea ice drift. SCATSAT-1 data is used as a primary data set to observe the D28 iceberg. Calving of D-28 was detected on 25 September 2019 (day no. 268 of 2019) from SCATSAT-1 data and SCATSAT-1 ceased to provide data on 3 March 2021 (day no. 062 of 2021). Our study covers the period from September 2019 to February 2021, and the dates are expressed in JD (Julian Day) (McCarthy, 1998).

Having a metre parabolic dish antenna with a dual feed assembly, SCATSAT-1 is a dual Ku-band pencil beam scatterometer. The conically scanning inner beam and the outer beam have swaths of 1400 and 1840 km, respectively. The inner beam is horizontally polarised, while the outer beam is vertically polarised. There are four levels of data products available from SCATSAT-1. The level-4, the enhanced products include sigma0, gamma0 and brightness temperature (at 2.25 km spatial resolution) in both horizontal and vertical polarisation (Singh, Singh, Maisnam, Jayaprasad, & Maity, 2019). Enhanced gamma0H (horizontally polarised gamma0) data sets are used as primary data to detect iceberg edges by applying the method discussed in Singh et al. (2021).

Accordingly, the Canny edge detection technique is applied to the gamma0H data with an upper limit, lower limit and Gaussian filter sigma of 0.4, 0.8 and 3.0, respectively, in Interactive Data Language (IDL) (Canny, 1986). These optimal values were arrived at after performing a series of several tests. From the detected edges, we manually identified the iceberg outline. The drift velocity of the iceberg was ascertained by measuring the rate of change of its position (metres per second, henceforth, m/s) in 24 h intervals. With a 5-day gap, 99 points of data of D28 iceberg locations were obtained from September 2019 to February 2021. The motion of the iceberg can be observed in Figure 1.

The ECMWF Reanalysis data version 5 or the ERA5 wind speed was used in this study. Hourly data of wind speed at 10 m above sea surface were downloaded from Copernicus ER5 (<https://cds.climate.copernicus.eu/>) (Hersbach et al., 2018). Hourly data in units of m/s were converted into daily average data. Only corresponding days mentioned in the previous subsection were chosen.

Next, the Ocean Surface Current Analysis Real-time (OSCAR) third-degree ocean surface current was also used. They were downloaded from Physical Oceanography Distributed Active Archive Center (PODAAC) (https://podaac-tools.jpl.nasa.gov/drive/_les/allData/oscar/preview/L4/oscar_third_deg) and provided daily average data in 5 days gap (ESR, 2009). The idea of using the 5-day gap in our study stemmed out from this data gap in the OSCAR data.

The sea ice concentration from the National Snow and Ice Data Center (NSIDC), University of Colorado, was used to ascertain sea ice conditions around the Antarctic waters. These data sets were downloaded from the NSIDC website (<https://nsidc.org/data/nsidc-0051>) (Cavalieri, Parkinson, Gloersen, & Zwally, 1996). To check the positive drag and negative drag of sea ice, we used Polar Pathfinder Daily 25 km EASE-Grid Sea Ice Motion (SIM) Vectors, Version 4, downloaded from the NSIDC website (<https://nsidc.org/data/NSIDC-0116>) (Tschudi, Meier, Stewart, Fowler, & Maslanik, 2019).

Wind, ocean current and SIM data are available in NetCDF format. A subsense of Antarctica, which contained the whole trajectory from September 2019 to February 2021, was cropped and extracted into point data (text format). The coordinates of D-28

for the corresponding days as observed from the SCATSAT-1 were identified from the subsense of the above three data sets. The data were extracted as feature points in the ArcGIS environment.

NSIDC sea ice concentration data are available in GeoTIFF format. Sea ice concentration values at locations of D-28 were extracted for the corresponding days as mentioned above.

Methodology

To study the effects of wind on iceberg motion, we follow the idea detailed in Wagner et al. (2017) that the drift velocity of an iceberg in strong wind conditions can be approximated by considering only 2% of the wind velocity relative to the ocean current. Typically, this rule is applicable around the Northern Hemisphere's icebergs. Wagner et al. (2017) applied this rule to the icebergs prevailing around the Antarctic Peninsula, but it was found that the iceberg motion was less affected by wind. The factors responsible for this behaviour could be due to smaller icebergs and weak wind conditions found during their observation. However, in the case of D28, which calved from the Amery Ice Shelf, the wind conditions were stronger than that in the east of Antarctic Peninsula (Yu et al., 2020).

A resultant vector between the ocean surface current velocity and "2% of wind velocity" (mentioned earlier) with its direction rotated at right angles anticlockwise was calculated to discuss the collective effect of both wind and ocean current on the motion of the iceberg. The process of rotation of wind velocity mentioned above is due to the Coriolis effect and is explained below.

Some of the wind drag is projected in the direction perpendicular to the wind velocity by the Coriolis effect (Wagner et al., 2017). The Coriolis force pushes icebergs anticlockwise in the Southern Hemisphere and clockwise in the Northern Hemisphere (Bigg, 2015). Wind drags, and Coriolis force becomes more important when ocean current velocity is weaker (Bigg et al., 1996).

For smaller icebergs (height less than 50 m and a horizontal length of around half a kilometre), the angle at which the surface winds drive the iceberg (relative to the direction of the wind) is calculated to be between 25° and 42° (Crépon et al. 1988). However, a more detailed discussion given in Wagner et al. (2017) discusses different deflection angles for different strengths of the wind. For strong winds, the deflection angle is about 0°, but for weaker winds, the deflection can be up to 90°. Thus, stronger winds drive the iceberg in the direction of the wind. It may also be noted that the shape of the iceberg affects the Coriolis force on the iceberg (Crépon et al. 1988). In Figure 1(a), the perimeter of the iceberg as detected by the Canny edge detector is shown in red, and the rotation of the iceberg in an anticlockwise direction is also visible. In our study, an anticlockwise rotation of 90° in wind direction was used to calculate the theoretical iceberg velocity. We chose this condition because most of the days showed weak wind speeds (less than 10 m/s) and weak ocean currents.

Results and discussion

From the statistical comparison between observed speed and resultant magnitude of the wind and ocean surface current, Pearson's correlation is found to be 0.32 (at 95 per cent confidence level) with RMSE 0.05 m/s. Ninety-nine days of observation from SCATSAT-1 are shown as green points in Figure 1(b). Of these, only 58 have no missing data in all SCATSAT-1 data, OSCAR

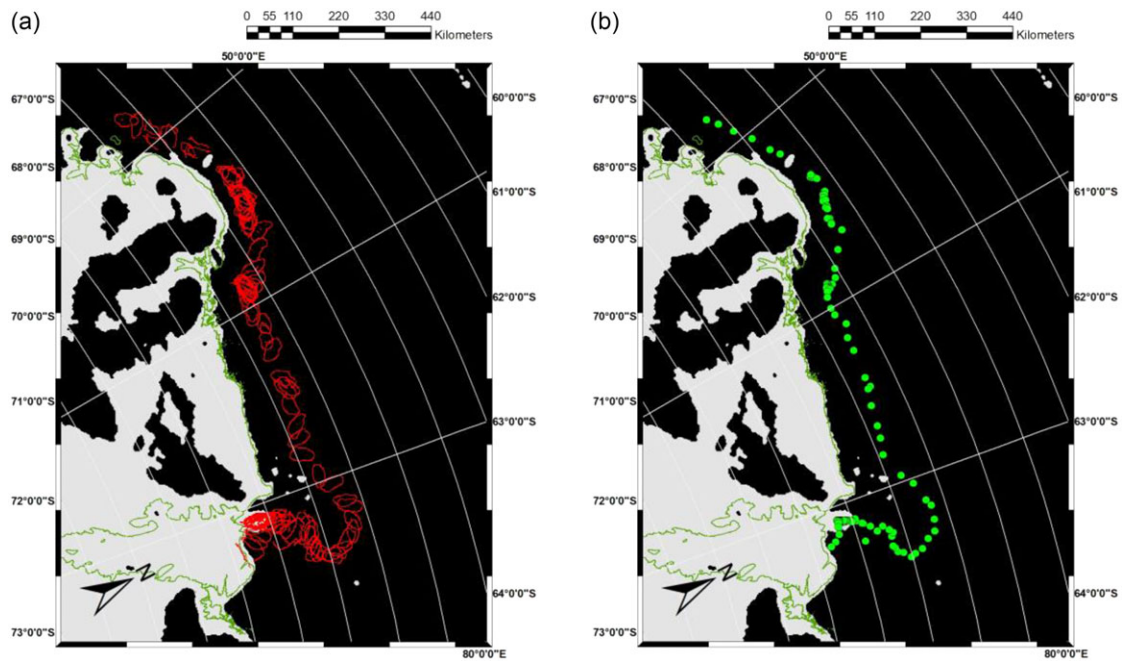


Fig. 1. (a) D28 movement detected from SCATSAT-1. (b) Observed positions for calculating iceberg velocity. The period of study is from September 2019 to February 2021. The background image is the classified image of SCATSAT-1.

ocean current data and ERA5 wind speed data. Using these 58 days, the above Pearson's correlation between the observed and theoretical is calculated.

The mean resultant speed was found to be 0.09 ± 0.04 m/s, whereas the observed speed was 0.08 ± 0.05 m/s. The difference in the speeds and their low correlation value is due to the exclusion of other towing forces (e.g. sea ice drag, basal melt, etc.). Figure 2 shows the time series plot of observed iceberg speed and resultant speed. Most of the days, both the observed and the resultant speeds were between 0.05 and 1.5 m/s.

The graphical plots of speed/velocity of the iceberg, wind, ocean, and sea ice speed versus time, and stick plot as time series are given in the Supplementary Material.

The time series of SIM data at the positions of the D28 iceberg is given in the Supplementary Material. There are data gaps due to the unavailability of the data and do not necessarily depict the absence of sea ice in the area which is ascertained from the sea ice concentration data (Fig. 3). The ice condition considered here is only for the regions around the different positions of the iceberg during its entire journey under study.

During the period of study, the D28 iceberg moved through the different climatic conditions of Antarctica, covering a distance of 1800 km (Approx.). Therefore, its trajectory is discussed by dividing it into five regions, as shown in Figure 4(a).

The overall direction during the motion of D28, starting from its calving to the termination of our study, was from east to west. However, in region 1, the iceberg moved in a northeast direction, and in regions 2, 3, and 4 it moved in the west direction. At the conjunction between regions 3 and 4, the iceberg moved around the northwest direction.

The directions mentioned above are approximate directions. When the iceberg's speed is very low, it is discovered that their direction in consecutive days is not truly along the approximate directions mentioned earlier. This can be explained as follows. The SCATSAT-1 data detect the edges of the iceberg with an error

of about 2.25 km, and the detected scene may contain noises from the surrounding ocean or sea ice. We, therefore, considered an average direction within a few days interval gap (5 days), in spite of knowing that it would yield a less accurate iceberg drift direction.

Speeds in regions 1, 3 and 4 were comparatively slower than those in regions 2 and 5. In region 1, there was a strong up-shore wind (average wind speed ~ 10 m/s), weak ocean current (0.01 m/s) and weak sea ice motion (0.06 m/s along the wind direction). Near the coastal area, ocean current data were not available. Yet, the overall movement showed that the iceberg moved against the wind and sea ice. It can be concluded that ocean currents and discharge mass from the Amery Ice Shelf pushed the iceberg away from the coastal area.

When the iceberg was far from the coast during JD 335 of 2019 to JD 077 of 2020 (austral summer), the sea ice concentration was below 50% (see Table 1 of Supplementary Material), the drag due to the sea ice got reduced, and the iceberg motion depended on the wind, the ocean current, and the Coriolis force. However, the speed of iceberg did not increase much.

It was observed in region 1 that out of the 22 data points in this period (austral summer), only 6 had the same direction of wind and ocean current ($-90^\circ < W < 90^\circ$) and the other 16 were in the range $90^\circ < W < 270^\circ$, where W is the angle between wind (considering Coriolis force) and ocean current.

When sea ice moves along with iceberg (the angle, θ , between the directions of the iceberg drift and sea ice motion, satisfies the inequality, $-90^\circ < \theta < 90^\circ$), it causes positive feedback in each other's velocities, whereas, when it moves against ($90^\circ < \theta < 270^\circ$), they slow each other (Hunke & Comeau, 2011). This means that even in the presence of sea ice, it may still be possible to increase the speed of iceberg drift significantly. The same feedback mechanism also applies to the resultant of the wind and the ocean current. Therefore, in region 2, the D28 iceberg moved with positive feedback from the sea ice (with an average concentration of 78%) from east to west, at a relatively faster speed

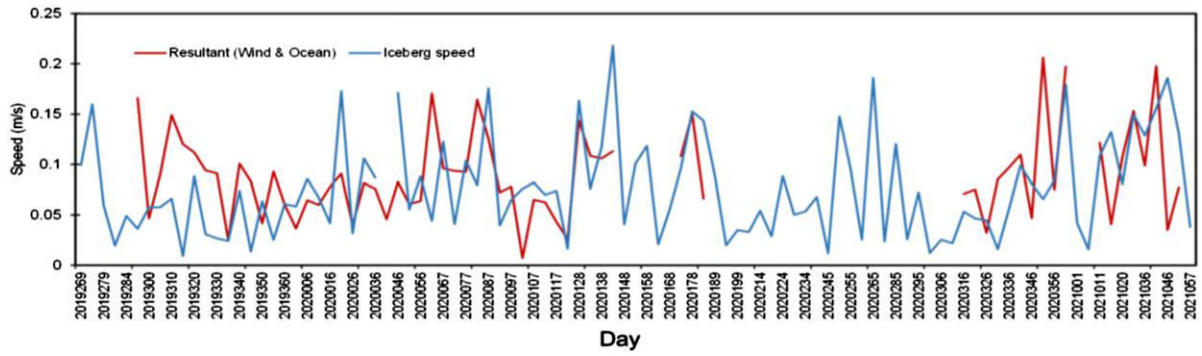


Fig. 2. Time series plot of resultant and observed speeds of D28 iceberg.

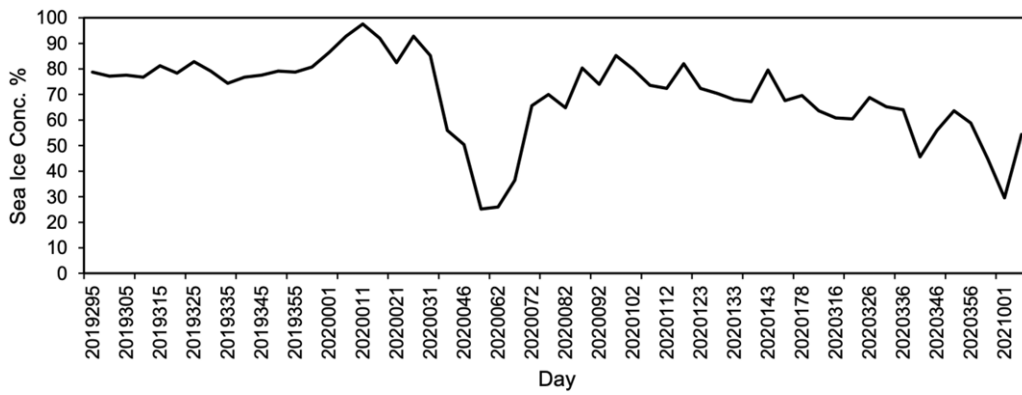


Fig. 3. Sea ice concentration.

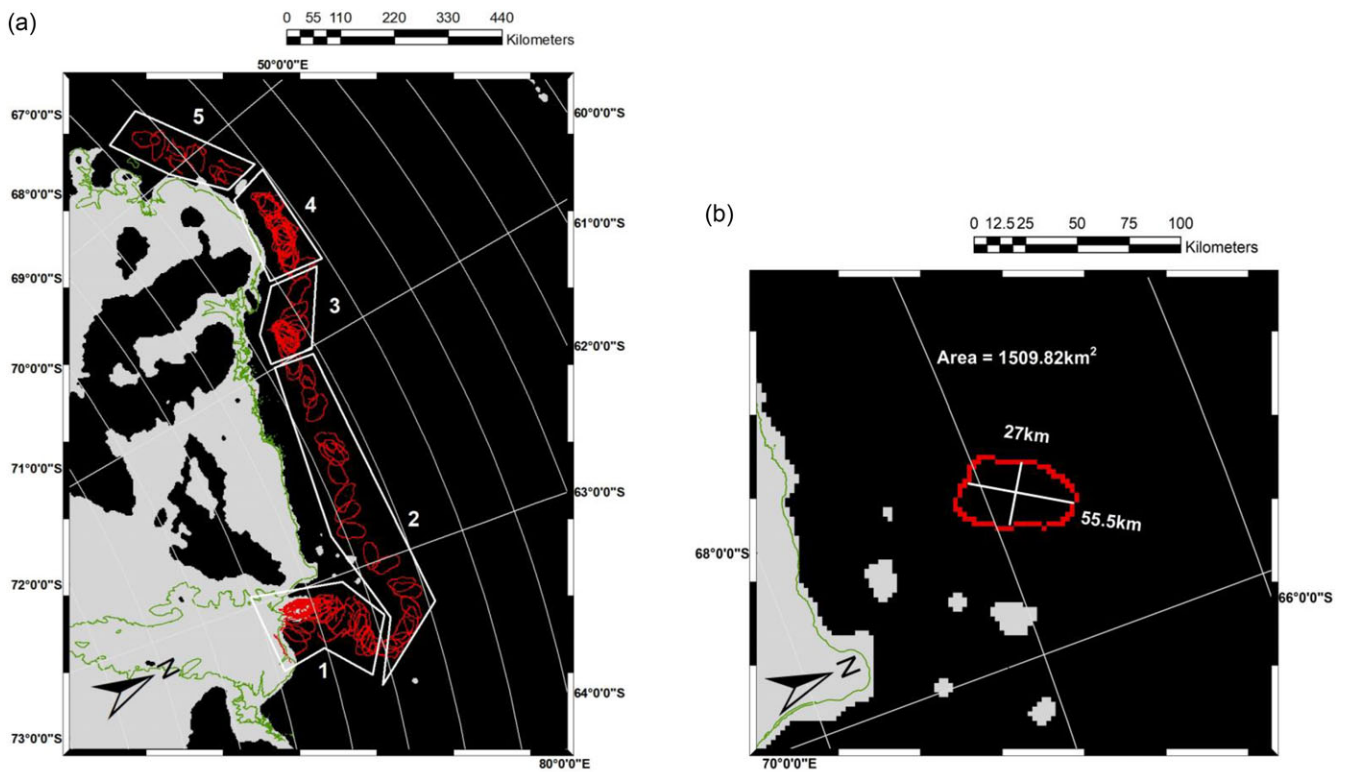


Fig. 4. (a) Location of regions used in Discussion. See text for details and (b) Size of D28 iceberg.

of 0.15 m/s. Since this period (JD 087 of 2020 to JD 184 of 2020) was in austral winter, ocean current data were not available for most of the points.

In region 3, from JD 194 of 2020 to JD 250 of 2020, sea ice motion was towards the east (i.e. against the motion of the iceberg) at 6 points out of 9 with an average speed of 0.08 m/s. Three out of 9 points with an average speed of 0.07 m/s moved towards the west. As such, negative feedback was given to the movement of the iceberg. The wind was also directed towards the east with an average speed of 5.1 m/s. Applying the Coriolis effect, the iceberg moved towards the coastal area, increasing the chance of it interacting with the higher sea ice concentration areas. Therefore, the iceberg slowed down under the influence of the thick sea ice (an average sea ice concentration of 88%).

In the conjunction between regions 3 and 4, the average iceberg speed increased to 0.09 m/s. From JD 255 of 2020 to JD 285 of 2020, sea ice concentration dropped (an average of 76%), but no ocean current data were available. Sea ice movement provided positive feedback (3 out of 3 points) to the direction of the iceberg. The direction of the wind was from the coastal area towards the ocean, and after applying the Coriolis effect (rotation of 90° anticlockwise), its direction gave positive feedback to the iceberg movement.

In region 4, for the period JD 290 of 2020 to JD 361 of 2020, (austral summer), most of the sea ice melted except for some near the coastline. In this region, average sea ice concentration dropped to 64%. However, the resultant of wind and ocean current provided negative feedback (8 out of 10 points) to the overall motion (east to west) of the iceberg. Thus, sea ice was not the only component slowing down the iceberg.

In region 5, from JD 001 of 2021 to JD 051 of 2021, sea ice concentration was low (<40%). Unfortunately, the 2021 sea ice movement data were not available at NSIDC's Polar Pathfinder website. Therefore, we approximated our calculation based on wind and ocean current only. During this period, at most of the points (5 out of 8 points), resultant of wind and ocean current gave a positive feedback to the iceberg motion.

Finally, from the on-screen digitisation of the shape of the iceberg in the ArcGIS environment, the average length and breadth of D28 were found to be 55.5 and 27 km, respectively (Fig. 4(b)). The total average area was found as 1509.82 km² (approx.). Iceberg areas were calculated from the average area of the detected iceberg edges using the ArcGIS polygon area calculation tool. It was calculated manually by drawing a polygon above the iceberg's edge. Open edges were discarded for this calculation.

Conclusion

Our aim in this study was to observe the motion of the iceberg D28 using SCATSAT-1. This motion is found to be influenced by various features such as the sea ice conditions, different atmospheric conditions (wind) and oceanic conditions (currents). Spatial and temporal behaviours of the iceberg could also be ascertained from the scatterometer data. We detected the edge of the iceberg, which was extensively used in the study of the geometric properties of the iceberg and its evolution through time.

With the help of wind, ocean current, sea ice concentration and sea ice motion data, we discussed the movement of the iceberg for the period from 26 September 2019 to 20 February 2021 (one and a half years). Using the four parameters above, we discussed the change in the speed and direction of the D28 iceberg.

From the digitisation of the iceberg, its average length and breadth were found to be approximately 55.5 and 27 km,

respectively. The average area was 1509.82 km². The average speed was found to be 0.08 ± 0.05 m/s, and it was moving in the east to west direction with an anticlockwise rotation.

Icebergs possess both destructive and productive power; therefore, their observation is important for shipping, sea bed structure planning and understanding the polar ecosystem. In recent years, the A-68 iceberg has threatened the island of South Georgia. Preventive measures can be taken by observing icebergs in such events.

Supplementary material. To view supplementary material for this article, please visit <https://doi.org/10.1017/S0032247423000062>

Acknowledgements. The authors would like to acknowledge the data sets from SCATSAT-1, ECMWF Reanalysis (ER5), OSCAR, NSIDC sea ice concentration and sea ice movement, and the data processing software (ArcGIS, ENVI and Python) used in this study. The authors would also like to acknowledge the anonymous reviewers who helped refine the article.

Financial support. This research received no specific grant from any funding agency, commercial or not-for-profit sectors.

Conflict of interest. The authors declare none.

Ethics of human subject participation. No human subject was used in this study.

References

- Ballantyne, J., & Long, D. G. (2002). A multidecadal study of the number of Antarctic icebergs using scatterometer data. In *IEEE international geoscience and remote sensing symposium*, Toronto, ON, Canada, vol. 5 (pp. 3029–3031). <https://doi.org/10.1109/IGARSS.2002.1026859>.
- Bigg, G. (2015). *The physics of icebergs*. In *Icebergs: Their Science and Links to Global Change* (pp. 52–81). Cambridge: Cambridge University Press. <https://doi.org/10.1017/CBO9781107589278.004>.
- Bigg, G.R., Wadley, M. R., Stevens, D. P., & Johnson, J. A. (1996). Prediction of iceberg trajectories for the North Atlantic and Arctic Oceans. *Geophysical Research Letters*, 23(24), 3587–3590. <https://doi.org/10.1029/96GL03369>.
- Canny, J. (1986). A computational approach to edge detection. *IEEE Transactions on Pattern Analysis and Machine Intelligence*, PAMI-8(6), 679–698. <https://doi.org/10.1109/TPAMI.1986.4767851>.
- Cavalieri, D. J., Parkinson, C. L., Gloersen, P., & Zwally, H. J. (1996). *Sea Ice Concentrations from Nimbus-7 SMMR and DMSP SSM/I-SSMIS Passive Microwave Data, Version 1*. Boulder, Colorado USA: NASA National Snow and Ice Data Center Distributed Active Archive Center. (Accessed on 04 December 2021). <https://doi.org/10.5067/8GQ8LZQVLOVL>.
- Crépon, M., Houssais, M.N., & Saint, G. B. (1988). The drift of icebergs under wind action. *Journal of Geophysical Research*, 93(C4), 3608–3612. <https://doi.org/10.1029/JC093iC04p03608>.
- ESR (2009). OSCAR third deg. Ver. 1. PO.DAAC, CA, USA. (Accessed on 06 December 2021). <https://doi.org/10.5067/OSCAR-03D01>.
- Hersbach, H., Bell, B., Berrisford, P., Biavati, G., Horányi, A., Muñoz Sabater, J., . . . Thépaut, J. N. (2018). *ERA5 hourly data on single levels from 1979 to present*. Copernicus Climate Change Service (C3S) Climate Data Store (CDS) (Accessed on 27 November 2021). <https://doi.org/10.24381/cds.adbb2d47>.
- Hunke, E. C., & Comeau, D. (2011). Sea ice and iceberg dynamic interaction. *Journal of Geophysical Research*, 116, C05008. <https://doi.org/10.1029/2010JC006588>.
- Lichey, C., & Hellmer, H.H. (2001). Modelling giant-iceberg drift under the influence of sea ice in the Weddell Sea, Antarctica. *Journal of Glaciology*, 47(158), 452–460. <https://doi.org/10.3189/172756501781832133>.
- Long, D.G. (2016). Polar applications of spaceborne scatterometers. *IEEE Journal of Selected Topics in Applied Earth Observations and Remote Sensing*, 10(5), 2307–2320. <https://doi.org/10.1109/JSTARS.2016.2629418>.
- McCarthy, D.D. (1998). The Julian and Modified Julian Dates. *Journal for the History of Astronomy*, 29(4), 327–330. <https://doi.org/10.1177/002182869802900402>.

- Misra, T., Chakraborty, P., Lad, C., Gupta, P., Rao, J., Upadhyay, G., ... Tolani, H. (2019). SCATSAT-1 Scatterometer: An improved successor of OSCAT. *Current Science*, 117(6), 941–949. <https://doi.org/10.18520/cs/v117/i6/941-949>.
- Oza, S.R., Bothale, R.V., Rajak, D.R., Jayaprasad, P., Maity, S., Thakur, P.K., ... Bahuguna, I.M. (2019). Assessment of cryospheric parameters over the Himalaya and Antarctic regions using SCATSAT-1 enhanced resolution data. *Current Science*, 117(6), 1002–1013. <https://doi.org/10.18520/cs/v117/i6/1002-1013>.
- Singh, K. N., Singh, R. K., Maisnam, M., Jayaprasad, P., Maity, S., Putrevu, D., & Misra, A. (2021). Detection of Two Recent Calving Events in Antarctica from SCATSAT-1. In *IEEE international geoscience and remote sensing symposium, IGARSS 2021* (pp. 439–442), <https://doi.org/10.1109/IGARSS47720.2021.9553306>.
- Singh, R.K., Singh, K.N., Maisnam, M., Jayaprasad, P., & Maity, S. (2019). Observing Larsen C ice-shelf using ISRO's SCATSAT-1 data. *Polar Science*, 19, 57–68. <https://doi.org/10.1016/j.polar.2018.12.007>.
- Singh, S., Tiwari, R.K., Gusain, H.S., & Sood, V. (2020). Potential applications of SCATSAT-1 satellite sensor: a systematic review. *IEEE Sensors Journal*, 20(21), 12459–12471. <https://doi.org/10.1109/JSEN.2020.3002720>.
- Singh, S., Tiwari, R.K., Sood, V., Kaur, R., & Prashar, S. (2022). The Legacy of Scatterometers: Review of applications and perspective. *IEEE Geoscience and Remote Sensing Magazine*, 10(2), 39–65. <https://doi.org/10.1109/MGRS.2022.3145500>.
- Smith, S. D., & Banke, E. G. (1983). The influence of winds, currents and towing forces on the drift of icebergs. *Cold Regions Science and Technology*, 6(3), 241–255. [https://doi.org/10.1016/0165-232X\(83\)90045-9](https://doi.org/10.1016/0165-232X(83)90045-9).
- Tschudi, M., Meier, W. N., Stewart, J. S., Fowler, C., & Maslanik, J. (2019). *Polar Pathfinder Daily 25 km EASE-Grid Sea Ice Motion Vectors, Version 4*. Boulder, Colorado USA: NASA National Snow and Ice Data Center Distributed Active Archive Center, (Accessed on 05 December 2021), <https://doi.org/10.5067/INAWUWO7QH7B>.
- Wagner, T. J. W., Dell, R. W., & Eisenman A. I. (2017). An analytical model of iceberg drift. *Journal of Physical Oceanography*, 47(7), 1605–1616. <https://doi.org/10.1175/JPO-D-16-0262.1>.
- Wesche, C., & Dierking, W. (2016). Estimating iceberg paths using a wind driven model. *Cold Regions Science and Technology*, 125, 31–39. <https://doi.org/10.1016/j.coldregions.2016.01.008>.
- Yu, L., Zhong, S., & Sun, B. (2020). The climatology and trend of surface wind speed over Antarctica and the Southern Ocean and the implication to wind energy application. *Atmosphere*, 11(1), 108. <https://doi.org/10.3390/atmos11010108>.